Unveiling trends in migration of iron-based nanoparticles in saturated porous media

Journal of Environmental Management 370 (2024) 122552

Contents lists available at ScienceDirect

Journal of Environmental Management

journal homepage: www.elsevier.com/locate/jenvman

Research article

Unveiling trends in migration of iron-based nanoparticles in saturated porous media

Veronika Veselská [a,*], Leonardo Magherini [b], Carlo Bianco [b], Jan Šembera [c], Petr Parma [c], Viktorie Víchová [a,d], Rajandrea Sethi [b], Jan Filip [a]

[a] Czech Advanced Technology and Research Institute, Regional Centre of Advanced Technologies and Materials, Palacký University Olomouc, Šlechtitelů 27, 783 71, Olomouc, Czech Republic
[b] Department of Environment, Land, And Infrastructure Engineering (DIATI), Politecnico di Torino, Corso Duca Degli Abruzzi 24, 10129, Turin, Italy
[c] Faculty of Mechatronics, Informatics and Interdisciplinary Studies, Technical University of Liberec, Studentská 1402/2, 461 17, Liberec, Czech Republic
[d] Department of Experimental Physics, Faculty of Science, Palacký University Olomouc, 17. Listopadu 1192/12, 779 00, Olomouc, Czech Republic

ARTICLE INFO

Keywords:
Zero-valent iron
Surface and chemical modification
Environmental remediation
Transport modelling

ABSTRACT

Nanoscale zero-valent iron (nZVI) particles are routinely used for environmental remediation, but their transport dynamics in different settings remain unclear, hindering optimization. This study introduces a novel approach to predicting nZVI transport in saturated porous model environment. The method employs advanced long column devices for real-time monitoring via controlled magnetic susceptibility measurements. Numerical modeling with a modified version of the MNMs 2023 software was then used to predict nZVI and its derivatives mobility in field-like conditions, offering insights into the radius of influence (ROI) and shape factor (SF) of their distribution. A standard nZVI precursor was compared with its four major commercial derivatives: nitrided, polyacrylic acid-coated, oxide-passivated, and sulfidated nZVI. All these iron-based nanoparticles exhibited identical particle sizes, morphologies, surface areas, and phase compositions, isolating surface properties, dominated by charge, as the sole variable affecting their mobility. The study revealed optimal transport when the surface charge of nZVI and its derivatives was strongly negative, while rapid aggregation of nZVI derivatives due magnetic attraction reduced their mobility. Modeling predictions based on column scale-up, indicated that detectable concentrations of 20 g L^{-1} were found at distances ranging from 0.4 to 1.1 m from the injection well. Slightly sulfidated nZVI traveled farther than the nZVI precursor and ensured more homogenous particle distribution around the well. Organically modified nZVI migrated the longest distances but showed particle accumulation close to the injection point. The findings suggest that minimal sulfidation combined with organic modification of nZVI surfaces may effectively enhance radial and vertical nZVI distribution in aquifers. Such improvements increase the commercial viability of modified nZVI, reduce their adverse impacts, and boosts their practical applications in real-world scenarios.

1. Introduction

Progress in nanotechnology over the past few decades has revolutionized environmental clean-up, enhancing traditional remediation methods with advanced nanoscale solutions. Among nanoscale materials, zero-valent iron (nZVI) particles offer unique remediation capabilities against various contaminants in groundwater and soils due to their exceptional reactivity, large surface area, and abundant reactive sites (Galdames et al., 2020; Latif et al., 2020; Pasinszki and Krebsz, 2020; Zafar et al., 2021). The potential benefits of nZVI nano-remediation over conventional technologies include fast and effective cleanup, broad applicability to various sites, and higher regulatory

Abbreviations: DLS, dynamic light scattering; EDX, energy-dispersive X-ray spectroscopy; LOI, length of influence; MNMs 2023, Micro and Nano-particles transport filtration and clogging Model Suite; N_nZVI, nitrided zero-valent iron nanoparticles; nZVI, zero-valent iron nanoparticles; Ox_nZVI, oxide-passivated nZVI; PA_nZVI, polyacrylic acid functionalized zero-valent iron nanoparticles; PA, polyacrylic acid; ROI, radius of influence; SEM, scanning electron microscopy; SF, shape factor; S_nZVI, sulfidated zero-valent iron nanoparticles; TEM, transmission electron microscopy; X_nZVI, unmodified zero-valent iron nanoparticles; XPS, X-ray photoelectron spectroscopy; XRD, X-ray powder diffraction.

* Corresponding author.
E-mail address: veronika.veselska@upol.cz (V. Veselská).

https://doi.org/10.1016/j.jenvman.2024.122552
Received 13 May 2024; Received in revised form 30 August 2024; Accepted 16 September 2024
Available online 8 October 2024

confidence. It is not invasive, easy to deploy, and less likely to harm sensitive water sources. Additionally, it can work well with biological methods and is effective in challenging conditions (Al-Hashimi et al., 2021; Karn et al., 2009; Li et al., 2014; Plessl et al., 2023; Sethi and Molfetta, 2019; Tosco et al., 2014a). However, nZVI-based nanoremediation still needs some optimization to deploy its full potential in contaminant removal. It is therefore essential to engineer nZVI to enhance targeted delivery and selectivity and boost its commercial relevance. This involves improving its chemical stability and minimizing water-induced surface passivation, which are crucial for increasing nZVI's reactivity and ensuring its long-term effectiveness against pollutants (Cheng et al., 2021; Eljamal et al., 2020; Jia et al., 2018; Liu et al., 2021; O'Carroll et al., 2013; Shan et al., 2021; Tian et al., 2020; Wu et al., 2020; Zhang et al., 2019).

Recent studies on environmental remediation have provided a deeper understanding of the complex behavior of nZVI in real-world conditions The mechanisms underlying nZVI's interaction with soil constituents and contaminants have been elucidated, providing insights into its long-term environmental impacts and sustainability (He et al., 2018; Keochanh et al., 2024; Visentin et al., 2024; Zhu et al., 2024). Moreover, a long term development of nZVI derivatives through surface alteration or composites on various matrices brought fruitful results in the form of successful applications in combination with bioremediation or electrokinetic remediation (Ahmad et al., 2023; Gao et al., 2025; Garcia et al., 2021; Ng and Lim, 2022; Nune et al., 2022; Velimirovic et al., 2020; Xu et al., 2024; Yusuf et al., 2024; Zhu et al., 2023). Different nZVI derivatives have been optimized to improve their reactivity, longevity and storage. As an example, advanced surface modifications, such as sulfidation and polymer or oxide coatings, have been tested in treating groundwater or mine waters contaminated with chlorinated hydrocarbons and metals, mainly with hexavalent chromium Cr(VI) (Dhanush Raj and Ahammed, 2024; Klimkova et al., 2011; Lacina et al., 2015; Li et al., 2014; Liu et al., 2024; Nunez Garcia et al., 2020a, 2020b; Semerád et al., 2021; Song et al., 2023; Stejskal et al., 2017; Su et al., 2019; Wang et al., 2024). Among them, sulfidation was proven as a successful methodology to obtain nZVI systems tailored for the effective degradation of chlorinated ethylenes (Bhattacharjee and Ghoshal, 2018; Brumovský et al., 2020; Cheng et al., 2024; Fan et al., 2016, 2017; Han and Yan, 2016; Lang et al., 2022; Wu et al., 2020; Xu et al., 2019, 2021). Sulfidated nZVI was favorably injected on a large scale at a site contaminated with organohalide pollutants, resulting in a rapid decrease in the concentration of volatile organic compounds in groundwater (Nunez Garcia et al., 2020a) and similarly for the reduction and immobilization of Cr(VI) in the aquifers (Brumovský et al., 2021).

Successful nanoremediation not only hinges on the reactivity of nZVI particles but also on their effective transport within the subsurface environment. Understanding the transport mechanisms that affect particle mobility in saturated porous media is crucial for improving the delivery of engineered nZVI in aquifers. This knowledge enables precise prediction and control of subsurface nZVI distribution, allowing for the effective design of injection strategies for in-situ aquifer remediation (Bianco et al., 2016, 2023; Mondino et al., 2020). To ensure efficient particle distribution within a contaminated aquifer, it is essential to optimize both the injectability and mobility of nZVI. This involves enhancing the injection area, minimizing pressure, and promoting even distribution of the particles (Tosco et al., 2014a). At the macro-scale, nZVI transport behavior is governed by physical and physicochemical interactions at the pore scale. These interactions are influenced by both the properties of the particles (size, shape, surface modification) and the characteristics of the porous medium (geology, granulometry) (Bradford et al., 2002; Pelley and Tufenkji, 2008; Seymour et al., 2013; Ting et al., 2021) Such interactions result in dynamic deposition and release phenomena, which directly affect nZVI mobility. Additionally, the transport of nZVI is affected by the rheological properties of the dispersant fluid and key hydrodynamic and hydrochemical parameters like pore water velocity, injection flow rate, ionic strength, and pH (Bradford and Torkzaban, 2008; Saleh et al., 2008; Tosco et al., 2009; Tufenkji and Elimelech, 2004). Together, these factors determine how effectively nZVI particles can move through and interact within the subsurface environment, impacting their overall mobility and distribution in remediation applications.

Despite the significant potential of nZVI in environmental remediation, detailed studies on its fate, transport, and associated toxicity remain underexplored. New methodological advancements offer promising perspectives for studying nZVI dynamics in real-time (Skácelová et al., 2020; Wu and Schwartz, 2020). However, the research gap lies in the lack of comprehensive investigations into the transport dynamics of nZVI and its various derivatives, coupled with the absence of standard testing methods to assess this transport effectively. Moreover, a comparison with previous studies on nZVI migration is challenging because of the diverse precursors and methods used in their preparation. Thus, this study aims to address these gaps by (i) uncovering trends in the migration of various nZVI derivatives using a uniform nZVI precursor, (ii) introducing an advanced column device for monitoring their transport, (iii) evaluating the role of surface chemistry in the mobility of nZVI and (iv) developing tools for predicting nZVI transport through scaling and predictive modeling. Indeed, the novel aspects of this research include the consistent synthesis of four nZVI derivatives: nitrided, organically modified with polyacrylic acid, air-stable with an oxidic shell, and sulfidated nZVI and the focus on the impact of surface modifications on their mobility. The hypothesis is that refining the surface treatment of nZVI will enhance its mobility and potentially minimize adverse effects. By selecting nZVI with tailored surface coatings, we focus on a critical factor that dictates their transport, stability, reactivity, and ecological footprint in remediation contexts. A combined experimental and modelling approach was applied to characterize and model the particle transport at the laboratory scale and foresee their behavior in field-relevant conditions. Both the quantitative interpretation of the laboratory scale experiments and the upscaled model predictions were performed with the help of the MNMs 2023 software (Micro and Nano-particles transport, filtration and clogging Model Suite), a numerical code specifically developed at Politecnico di Torino for the simulation of particle transport in saturated porous media. The findings of this study intend to guide precise adjustments to nZVI surfaces, improving its movement in specific environmental contexts. Such enhancements could improve nZVI's practical applications and reduce any negative impacts, thereby benefiting both environmental remediation practices and public health.

2. Material and methods

2.1. nZVI derivatives

Previously well-documented and commercially available nZVI was selected as the basic type (as a reference) of nanoparticle and used as a precursor for other modifications in this study (Table 1). Pyrophoric metal powders of unmodified (labeled X_nZVI) and oxide-passivated nZVI (labeled Ox_nZVI) were purchased from NANO IRON s.r.o, Czech Republic (NANOFER 25P and NANOFER STAR, respectively). Nitrided N_nZVI was synthesized via the incorporation of atomic nitrogen throughout the entire volume of nZVI (NANOFER 25P), resulting in the formation of crystalline forms of γ′-Fe nitrides. N_nZVI particles were prepared using a nitriding gas mixture with a composition of NH_3: N_2 in a 1:2 ratio. The gas flow rate was maintained at 30 L h^{-1}. The reaction was carried out at a temperature of 500 °C for 3 h (Brumovský et al., 2022, 2023). The organically modified nZVI was freshly prepared from NANOFER 25P by surface-functionalization with organic molecules of polyacrylic acid (Klimkova et al., 2011) and labeled as PA_nZVI. Sulfidated S_nZVI with various S/Fe mass ratios (0.005, 0.01, 0.02, and 0.05) were prepared by applying inorganic sulfur-based coatings to nZVI (NANOFER 25P). These mass ratios were selected in accordance with the detailed previous study on the reactivity of these materials (Brumovský

Table 1
Summary of nZVI-based derivatives.

nZVI	Commercial production	Type of modification	nZVI	Commercial production	Type of modification
X_nZVI	NANOFER 25P 409	unmodified	S_nZVI_0.5	–	sulfidated S/Fe = 0.005
N_nZVI	–	nitrided	S_nZVI_1.0	–	sulfidated S/Fe = 0.01
PA_nZVI	–	organic surface layer	S_nZVI_2.0	–	sulfidated S/Fe = 0.02
PA_nZVI_com	NANOFER 25S	organic surface layer	S_nZVI_5.0	–	sulfidated S/Fe = 0.05
Ox_nZVI	NANOFER STAR 586	oxid surface shell	S_nZVI_com	NANOFER 25DS	Fe sulfide surface layer

et al., 2020). For comparison, two other nZVI samples were purchased from NANO IRON s.r.o, Czech Republic: NANOFER 25S (polyacrylic acid modified nZVI) and NANOFER 25DS (sulfidated nZVI), here labeled as PA_nZVI_com and S_nZVI_com, respectively (Table 1). Additional details of the nZVIs preparation and characterization are provided in the Supplementary Information (SI, chapter 1 and Table S1).

Concentrated suspensions of nZVI (250 g L^{-1}) were prepared by dispersing the nanoparticles in a high-speed homogenizer (ULTRA-TURRAX IKA T18 [S18N-19G], IKA, Staufen, Germany) for 2 min at 11,000 rpm in 50 mL of tap water (Table S2). Tap water served as a better model than demineralized or ultrapure water due to its closer resemblance to natural water systems in terms of ionic strength, pH, mineral content, and biological components. The suspensions were subsequently diluted to a concentration of 5 g L^{-1} and dispersed for 15 min at 15,000 rpm in a final volume of 2 L. To restore the reactivity of Ox_nZVI, an activation procedure was conducted prior to migration experiments (Ribas et al., 2017). The initial Ox_nZVI suspension was kept in tap water for 48 h at room temperature (23 °C), followed by re-suspension and dilution to the final concentration.

All the nZVI derivatives were analyzed to quantify their surface area (S_{BET}), size distribution, and surface charge, composition and morphology. The Brunauer-Emmett-Teller method (BET; Autosorb iQ XR, Anton-Paar Quanta Tec, USA) was utilized to determine the surface area. The elemental composition of the nZVI derivatives' surfaces was further characterized using X-ray photoelectron spectroscopy (XPS; VersaProbe II, Physical Electronics Inc, USA). Energy-dispersive X-ray spectroscopy (EDX; ThermoFisher Scientific, USA) coupled with scanning electron microscopy (SEM; ThermoFisher Scientific, USA) was employed to analyze the qualitative elemental composition and surface morphology of the samples. Dynamic light scattering (DLS; Zetasizer Nano ZS, UK) was used to measure the zeta potential and, together with transmission electron microscopy (TEM; JEM 2100, JEOL Ltd., Japan), to evaluate the particle size distribution. For modeling purposes, the size distribution and surface charge were also measured for suspensions diluted prior to the migration experiments. The phase compositions of the suspensions of nZVI derivatives were determined using X-ray powder diffraction (XRD; Malvern PANalytical, USA). The crystallographic structural parameters and crystallite sizes (D_{cryst}) of the identified phases were calculated using Rietveld refinement (all details are provided in the SI, Chapter 1 and Table S1).

2.2. Migration experiments

The experimental setup which was used to test the nZVI particle migration comprised a 2 m long polymethylmethacrylate column with an internal diameter of 2 cm, vertically dry packed with a technical quartz sand (Sklopísek Střeleč, ST05/10, Czech Republic, d_{50}, of 0.76 mm, bulk density ρ_b, of 1.5 kg L^{-1}) (Fig. 1). Presented setup was deemed optimal for minimizing boundary effects due to uniformity of the sand while maintaining manageable material usage and ensuring reliable data collection and precise replication of real-word conditions (Brumovský et al., 2021; Černík et al., 2019; Němeček et al., 2016; Parma et al., 2020). Sandy porous medium was used for tracking nZVI transport because it provides a uniform and controlled environment, allowing for consistent and reproducible results. This standardization helps isolate the effects of nZVI behavior from the variability inherent in real soil, making it easier to interpret and compare data (Molnar et al., 2016; Shen et al., 2024; Wei et al., 2024). Using sand with grain sizes between 0.5 and 0.8 mm ensures optimal nZVI mobility by balancing hydrodynamic resistance and pressure. Smaller grains could cause clogging and increased inlet pressure, while larger grains may allow nZVI to pass too quickly without sufficient retention.

The dry sand was carefully poured into the column, and periodic tapping was done on the column sides to ensure even distribution. The column was subsequently flushed with CO_2, followed by at least one pore volume of tap water to expel the CO_2 and guarantee saturation. The porosity was directly calculated by measuring the amount of tap water required to fill the pore volume (Table S3) before each experiment, with

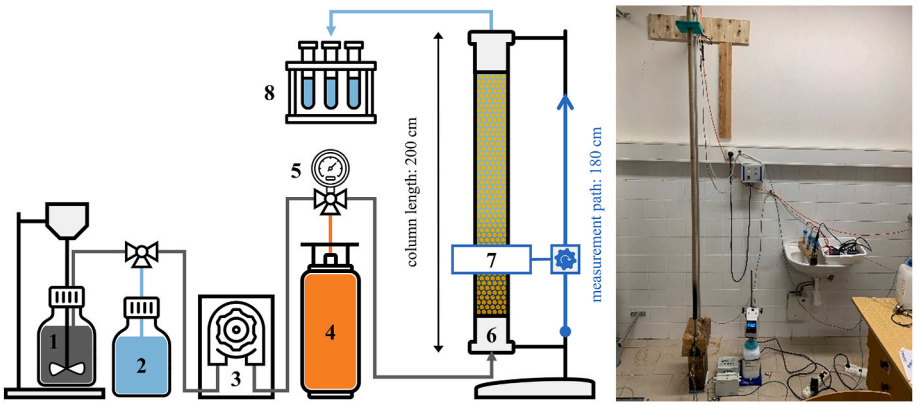

Fig. 1. Column set up: shaft-driven stirred nanoparticle suspension vessel (1); tap water vessel (2); peristaltic pump (3); CO_2 gas cylinder (4); three-way valve and manometer (5); column (6); coil for ferromagnetic susceptibility measurement with stepper motor (7); flow cells with electrodes for measuring Eh, pH, and conductivity (8).

an average value of 39.9%. The nZVI suspensions (5 g L^{-1}), which were continuously stirred using a shaft agitator (WiseStir HS-30D, Witeg, Germany) at 500 rpm, were pumped using a peristaltic pump (ISMATEC IPC, Masterflex, USA) from a storage vessel into the column at a stable flow rate of 10 mL min^{-1} (Darcy velocity of 3.18 cm min^{-1}) for 2 h, corresponding to approximately 5.6 pore volumes. The flow inside the column was vertical and upward. The column was then flushed with tap water for 2 h to evaluate the particle detachment rate. During nZVI suspension injection and tap water flushing, the pH, Eh, and conductivity parameters were constantly monitored in the column effluent (Fig. S1), and the pressure was measured at the column inlet to detect potential porous media clogging. The nZVI concentration along the column was periodically scanned using a coil for the ferromagnetic susceptibility measurements. Tracer tests were conducted with a NaCl solution to measure the conductivity at the inlet and outlet of the column. The dispersity was then determined from one of the tracer tests and was assumed to be equal to 0.5 mm for all column tests (Fig. S2).

2.3. Ferromagnetic susceptibility measurement and data processing

Magnetic susceptibility measurements were conducted to detect changes in the oscillator frequency, corresponding to alterations in the magnetic susceptibility of the model porous medium. During the 2-h migration experiment, a motorized detection coil (ID 32 mm, 200 wire turns, height 8 mm) scanned the column every 10 min, taking 180 measurements at 1 cm intervals. The ferromagnetic susceptibility was measured using a resonant circuit with constant capacitance, where coil inductance depended on the surrounding susceptibility (see details in SI, chapter 2). The basic measurement frequency was 3.6 kHz. To prevent aggregation of ferromagnetic nanoparticles due to secondary magnetization, a low-intensity magnetic field (≈6 mT) was used (Parma et al., 2020; Vecchia et al., 2009a).

The scanning process began at the top of the column (180 cm from the bottom) for calibration, with the detector moving to the bottom and measuring every centimeter for 2.65 s as it moved upward. First, background measurements were obtained from multiple saturated column scans. Then, suspension injection began with the initial coil measurement taken at the base of the column. One column experiment resulted in 12 scans analyzed using "ZVFE" software 2015. Raw frequency data processing involved three steps: (i) subtracting background noise and correcting for temperature-induced signal drift; (ii) deconvoluting the data to isolate the elementary iron signal, using a set of linear equations to solve for the deconvolved frequencies; (iii) converting the deconvolved frequencies into nZVI concentrations using conversion constants which slightly varied with the specific surface modification of nZVI (Fig. S3). A detailed description and values of these constants are provided in the SI, chapter 3 and Table S3. To obtain input data for the modeling software, we used linear interpolation to convert concentrations from multiple scans into a single time frame. This process involved using a weighted average to calculate the concentrations at the desired time based on the closest two scans in the same column segment.

2.4. Transport modeling of migration experiments

The transport of nZVI was modeled using a modified version of the MNMs 2023 software (Micro- and Nanoparticle transport, filtration, and clogging Model-Suite, r. 4.011a) (Bianco et al., 2016, 2017). The experimental retention profiles were fitted simultaneously using the Levenberg–Marquardt method for nonlinear least squares. The mobility of nZVI was assessed using a finite difference approach applied to a modified advection-dispersion equation, which describes the dual-phase kinetic interactions between the liquid and solid phases (Bianco et al., 2016; Pulido-Reyes et al., 2022):

$$\begin{cases} \varepsilon\dfrac{\partial C}{\partial t}+\sum_i \rho_b\dfrac{\partial S_i}{\partial t}+q_x\dfrac{\partial C}{\partial x}-\varepsilon D_x\dfrac{\partial^2 C}{\partial x^2}=0 \\ \rho_b\dfrac{\partial S_i}{\partial t}=\varepsilon k_{a,i}f_{a,i}C \end{cases} \quad \text{(Eq 1)}$$

where ε is the porosity of the porous medium $(-)$, ρ_b is the bulk density of the porous medium (kg m^{-3}), q_x is the Darcy flow velocity along the x coordinate (m s^{-1}), and D_x is the hydrodynamic dispersion coefficient (m^2 s^{-1}). This was calculated as $\alpha_x\frac{q_x}{\varepsilon}$ where α_x is the dispersivity (m). The concentration of nZVI was divided between those suspended in the liquid phase C (kg m^{-3}) and those retained on the porous medium S (kg kg^{-1}). The subscript i refers to the multiple concurrent interaction mechanisms between the particles and porous media. The attachment coefficient $k_{a,i}$ regulates the particle deposition rate (s^{-1}) while $f_{a,i}$ is a generic function that depends on the case-specific deposition mechanism. This function is equal to one for the linear attachment process. It adopts the form $\left(1-\frac{S}{S_{max}}\right)$ for a blocking mechanism where S_{max} represents the maximum number of particles that can be retained on the solid phase under specific chemical conditions (Ko et al., 2000; Ko and Elimelech, 2000). For modeling a straining mechanism, the function is expressed as $\left(1+\frac{x}{d_{50,s}}\right)^{-\beta_{str}}$, where $d_{50,s}$ is the average porous media diameter (m) and parameter β_{str} controls the shape of the particle spatial distribution $(-)$ (Bradford et al., 2002; Raychoudhury et al., 2014).

2.5. Radial injection simulations – ROI and SF integration

The permeation injection of nZVI through a screened well into a homogeneous and isotropic aquifer was simulated using a one-dimensional scenario, assuming radial symmetry and negligible influence of the groundwater background velocity on the overall flow field:

$$\begin{cases} \varepsilon\dfrac{\partial C}{\partial t}+\sum_i \rho_b\dfrac{\partial S_i}{\partial t}+\dfrac{1}{r}\dfrac{\partial}{\partial r}(rq_rC)-\dfrac{\varepsilon}{r}\dfrac{\partial}{\partial r}\left(rD_r\dfrac{\partial C}{\partial r}\right)=0 \\ \dfrac{\partial}{\partial t}(\rho_b S_i)=\varepsilon k_{a,i}f_{a,i}C \end{cases} \quad \text{(Eq 2)}$$

where r is the radial coordinate describing the distance from the injection point (m) and, D_r is the dispersion coefficient (m^2 s^{-1}) calculated as $\alpha_r\frac{q_r}{\varepsilon}$. Under the radial flow regime, the Darcy flow velocity $q_r=\frac{Q}{2\pi r}$ (m s^{-1}) depends only on the injection flow rate and well geometry, and it decreases hyperbolically with increasing distance from the injection well. Q represents the injection discharge rate per well screen unit (m^2 s^{-1}). Because the particle deposition rate is strongly influenced by the flow velocity (Li et al., 2008), the formula proposed by (Tosco et al., 2014b) was employed in this study to model the influence of velocity on the attachment coefficient $k_{a,i}$:

$$k_{a,i}(q_r)=C_{a,i}\frac{q_r}{\varepsilon\, d_{50,s}}\eta_0(q_r) \quad \text{(Eq 3)}$$

where $C_{a,i}$ $(-)$ is an empirical coefficient determined by fitting the experimental data (Bianco et al., 2017). $\eta_0(q_r)$ is the single collector contact efficiency $(-)$, which describes the effect of different deposition mechanisms (gravitational sedimentation, interception, and Brownian diffusion) on the particle transport under specific assumptions and simplifications (single spherical collector, infinite fluid domain, and uniform flow field) (Yao et al., 1971) (detailed information can be found in SI, chapter 4, Tables S4 and S5 and Fig. S4). In this study, a simplified procedure, described in details in SI (chapter 5), was applied to estimate $C_{a,i}$ from the results of the single-column tests performed at a constant

velocity (Table S4) (Pulido-Reyes et al., 2022). The transport of nZVI in radial symmetry was numerically solved using the MNMs 2023 software, simulating the injection of 1 m^3 of nZVI suspension with a concentration of either 5 g L^{-1} or 10 g L^{-1} at a flow rate of 1 m^3 h^{-1} (Tosco et al., 2014b), through a 4″ well screened in an aquifer with the same characteristics as the column tests. The radius of influence (ROI) was defined as the radial distance from the injection well where a particle concentration of at least 5 g kg^{-1}, corresponding to a C_{TOT} of 20 g L^{-1} of pore volume, was predicted. The ROI of nZVI was compared with the ROI of the tracer, calculated as $\sqrt{V/\pi\epsilon}$, where V is the injected volume per well screen unit (m^2). The dispersion of nZVI particles was defined using the shape factor (SF), which describes how the nZVI particles are distributed around the center of the well, offering insight into their dispersal patterns:

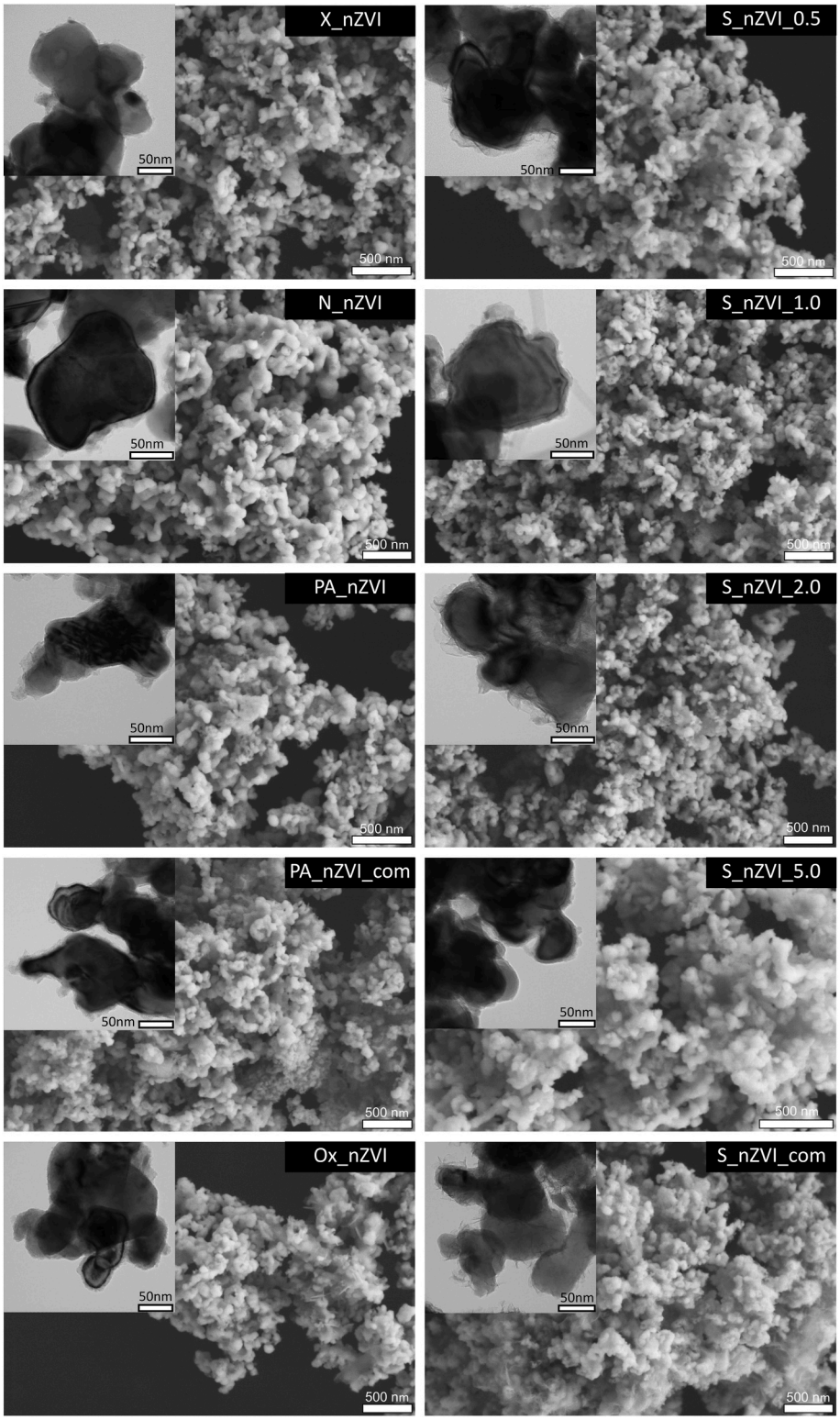

Fig. 2. Transmission electron microscopy (TEM; smaller images) and scanning electron microscopy (SEM; larger images) of various nZVI derivatives.

$$SF = 2\pi\varepsilon H \int_0^{+\infty} C_{TOT} r^3 dr \quad \text{(Eq 4)}$$

where H is the well screen height (m), and C_{TOT} is the total particle concentration per unit of pore volume (kg m^{-3}), calculated as the sum of the concentrations of suspended and retained particles (see details in the SI, chapter 6).

3. Results and discussion

3.1. Features of nZVI and its derivatives

All nZVI derivatives used in this study exhibited spherical particles with an average size ranging between 49 and 67 nm and a specific surface area of 24 m^2 g^{-1}. Based on Scherrer's equation, the synthesized nZVI derivatives had a crystalline size of α-Fe ranging from 35 to 68 nm, which matched well with TEM observation (Fig. 2; Fig. S5, and Table S1). Surface modification of the nZVI precursor resulted in derivatives with a negative surface charge and a distinctive surface morphology, where a dense iron core is encased in an oxide shell composed of FeO and Fe_3O_4, as confirmed by XRD, SEM-EDX, and TEM analyses (Fig. 2, Figs. S5 and S6 and Table S1). The oxide content in the derivatives ranges from approximately 1.6 to 6.8 wt% (Table S1). All nZVI derivatives, regardless of modification, consistently formed microscale aggregates up to 5 μm, as shown by DLS and SEM (Fig. 2, Table S1). This aggregation is likely due to effective collisions in the highly concentrated suspensions (25% w/v nZVI), which promote the formation of these aggregates.

The impact of surface modification was further evident in the composition measured in 2–5 nm probing depth on surface, as shown by XPS measurements (Table S1). The survey XPS spectra revealed two main peaks corresponding to iron (Fe 2p, 8.5−14.5 at.%) and oxygen (O 1s, 40−59.6 at.%), with additional elements such as sulfur (S 2p, 0.1−8.8 at.%) in S_nZVI and nitrogen (N 1s, 2.7 at.%) in N_nZVI, indicating the influence of different surface treatments. Moreover, the phase composition analysis by XRD showed that all derivatives contained more than 90 wt% of crystalline α-Fe, except for N_nZVI, which was predominantly composed of Fe_4N (96.9 wt%) (Table S1).

Results of material characterization imply that the modifications applied to precursor nZVI (i.e., X_nZVI) minimally impacted size and shape of aggregates and is fully consistent with previous studies published on detailed characterization of respective particles (Brumovský et al., 2020, 2021, 2022, 2023; Filip et al., 2014; Kašlík et al., 2018; Semerád et al., 2020; Soukupova et al., 2015). However, magnetic nature of nZVI derivatives and negative surface charge could contribute most significantly to their mobility. The magnetic interactions among nZVI particles often lead to aggregation, which hinders their mobility in porous media. Nanoparticles behave like permanent magnetic dipoles attracting each other due to magnetic interactions, which typically prevail above all the other surface repulsive forces acting on nZVI, i.e. electrostatic forces (Fazeli Sangani et al., 2019; Rosická and Sembera, 2011; Vecchia et al., 2009b; Xie et al., 2024). Previous studies confirmed that the aggregation rate of nZVI increases when increasing particle concentration and saturation magnetization (Kocur et al., 2013). The rapid formation of large aggregates significantly influences nZVI mobility, causing their settlement and possible deposition in porous media because of the enhanced straining mechanism (Kuyukina et al., 2022; Ling et al., 2021; Ng and Lim, 2022). However, when primary nanoscales gather to form microscale aggregates, they lose their magnetic properties due to the random arrangement of single dipoles. Rosická and Sembera (2011) showed that the magnitude of magnetic interactions among aggregates decreases with increasing the number of particles forming the aggregate. Under such conditions, other interaction mechanisms including electrostatic repulsion, may also play a relevant role in particle-particle interactions. In this study DLS measurement showed that N_nZVI, Ox_nZVI, PA_nZVI, and S_nZVI all possess negative surface charges, with zeta potentials ranging from −6 mV for Ox_nZVI to −41 mV for PA_nZVI. This values suggest that repulsive aggregate-aggregate interactions may be relevant for the studied particles and can contribute to improve nZVI mobility during transport in porous media due to the occurrence of blocking mechanisms (Ling et al., 2021). The hypothesis of possible blocking mechanisms during aggregate transport was also confirmed by transport modelling (see section 3.3). Additionally, the presence of an oxide shell (FeO and Fe_3O_4) on the surface of the nZVI derivatives further impacts electrostatic interactions by altering the surface chemistry, which plays a crucial role in the particle's overall mobility in environmental remediation applications (Dong and Lo, 2014; Mackenzie and Georgi, 2019; Su et al., 2020).

Although the magnetic properties of nZVI may hinder its mobility, they also enable efficient detection using electromagnetic induction sensors owing to changes in magnetic susceptibility. Thus, the column setup presented in this study may provide suitable feedback for the spatial and temporal migration of nZVI in space and time.

3.2. Insights from column tests

The deposition profiles of nZVI measured across different locations and times provided more details on nZVI transport than typical short-column breakthrough experiments (Bianco et al., 2016; Chen et al., 2023; Liu et al., 2019; Vecchia et al., 2009a). The deposition profiles for all tested nZVI in porous media showed a consistent pattern: the concentration increased with time at a set distance from the injection point, whereas it decreased along the column length moving away from that point (Fig. 3). Notable differences in the concentration profiles were observed across the various nZVI tests, indicating distinct retention and migration characteristics for each nZVI type. For clarity, among multiple replicates performed in each column experiment (Fig. S7), only a single representative profile was chosen that best reflects the average behavior observed across all replicates (Fig. 3). To ensure the accuracy of the analysis and modeling, the initial 10 scans from each deposition profile were utilized to reduce the effect of potential nZVI column breakthroughs.

The ongoing reactions of iron with water did not influence the change in the measured signal during the short time interval of the experiment, thus eliminating the need for more effective measurement methods to predict transport distances. The accuracy and sensitivity of the ferromagnetic measurement were verified by their repeatability (results not shown) and are confirmed by the consistency of the measured signal throughout the experiment itself, including the elution phase. The mass balance data indicated that very low levels of nZVI passed through the column, demonstrating efficient retention (Fig. S8). During the initial scans of the flush phase, minimal nZVI movement was observed; however, no further nZVI detachment occurred. This also confirmed the stable retention of nZVI under the experimental conditions. Moreover, the physicochemical parameters across all the nZVI tests showed consistent trends, revealing steady suspension properties (Fig. S1). Additionally, the observed small pressure changes were limited to 45 kPa, which is the evidence of minimal risk of column clogging.

To measure how nZVI affected their environment in the column, the Length of Influence (LOI) was established for this study. The LOI was defined as the distance from the injection point to the position where the C_{TOT} reaches 20 g L^{-1} of pore volume, equivalent to 5 g kg^{-1} of soil, as observed in the final scan. While ROI provides a measure of the extent of influence in a circular or spherical radius around the source point, LOI is directional and provides information on the spread of the effect in a particular direction. Moreover, LOI can indicate the preferential pathways of nZVI flow and transport, essential for targeted remediation and understanding the impact on downstream areas.

For unmodified X_nZVI, the four-column tests revealed significant variations in the concentration profiles despite all presenting a sigmoidal shape (Fig. 3). These differences may be attributed to different

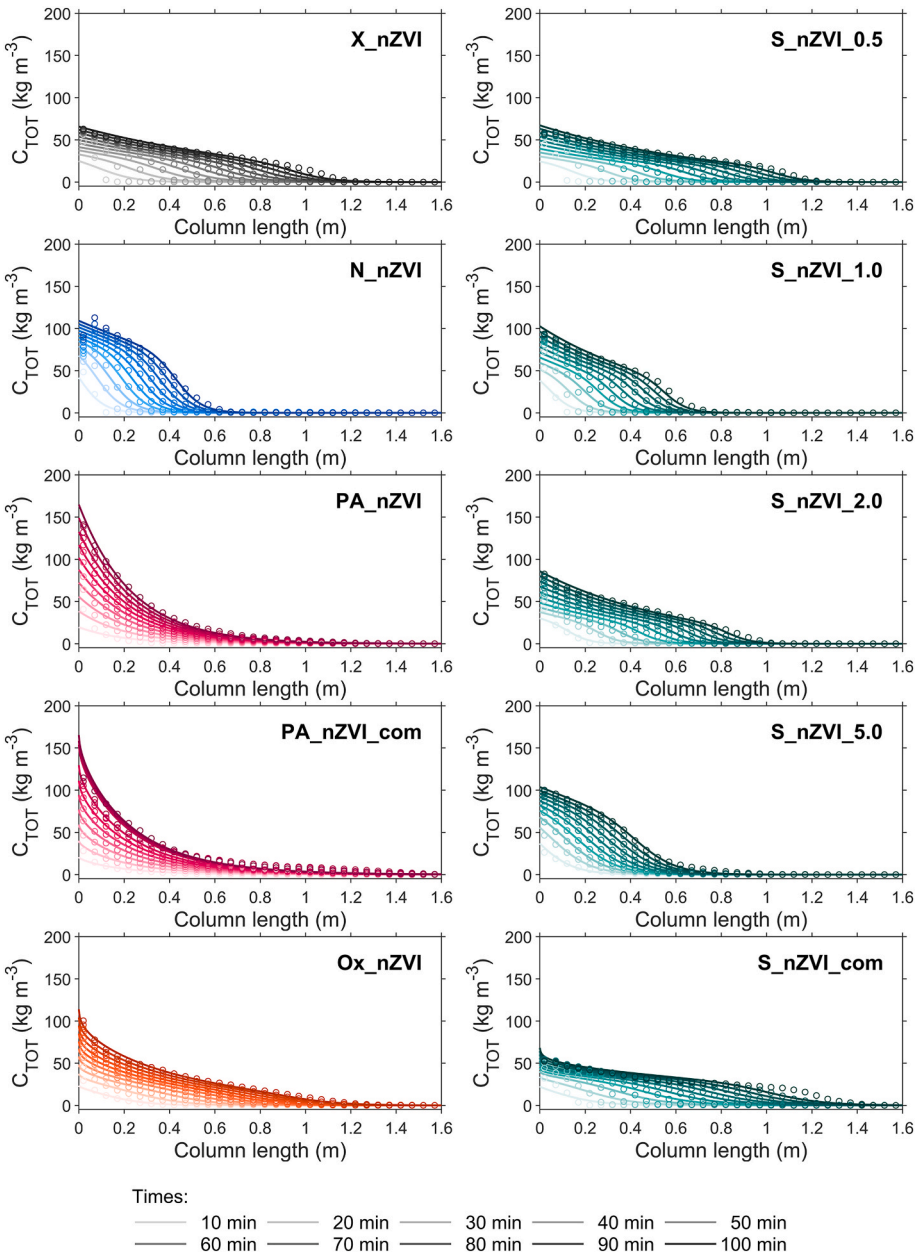

Fig. 3. Concentration profiles of unmodified X_nZVI and its derivatives; symbols and lines represent experimental and modeled data in time, respectively.

aggregation rates during suspension preparation. The longest distance of X_nZVI achieved during a 100-min timeframe (analogous to 10 scans) fluctuated between 0.5 and 1.5 m, and LOI ranged between 0.45 and 1 m, highlighting the diverse behavior of X_nZVI in terms of migration capabilities. Similarly, the shape of the N_nZVI concentration profiles and variations of LOI (0.44–0.88 m) were like those of X_nZVI. Organically modified PA_nZVI, PA_nZVI_com, and Ox_nZVI with oxide shells exhibited (hyper)exponential concentration profiles with a significantly higher C_{TOT} at the column inlet than X_nZVI. Increasing the viscosity using organic stabilizers resulted in enhanced mobility, as previously observed for carbon-based nanoparticles (Bianco et al., 2016). Although organic modification allowed nZVI to achieve the longest distances (1.1–1.7 m), LOI was within the same intervals as for the others, reaching 0.5–0.86 m, representing only approximately 50% of the total migration distance observed. Ox_nZVI reached an LOI of 0.5–0.7 m. Transport of S_nZVI was influenced by the degree of sulfidation. nZVI exhibiting a minimal degree of sulfidation, S_nZVI_0.5, S_nZVI_1.0, and S_nZVI_com, demonstrated comparable or slightly enhanced mobility compared to X_nZVI (1–1.3 m). S_nZVI_com achieved the furthest migration (up to 1.5 m), with an LOI exceeding 1 m, indicating its superior dispersal capability. Sulfur content above 1% slightly decreased the total migration distance and LOI, leading to higher nZVI accumulation at the inlet of the column. In this study, X_nZVI and all the tested derivatives exhibited comparable migration distances and LOI, with a consistent detection concentration of 20 g L^{-1} achievable between 0.4 and 1.1 m. Despite these similarities, the spatial and temporal distributions of individual nZVI modifications varied, indicating distinct underlying transport mechanisms.

3.3. *Migration mechanisms*

One- or two-site attachment models were selected to fit the column experimental results assuming no particle detachment (Boccardo et al., 2020; Tosco et al., 2009; Tosco and Sethi, 2009). The choice of a specific model was customized to each nZVI derivative based on the various shape of its concentration profile curve and fitting success of different

models. Exponentially decreasing profiles showed best fit using linear deposition models, sigmoidal curves were best fitted using the blocking mechanism, and hyper-exponential profiles most accurately modeled by straining model. A combination of these models has been appropriate for profiles with more complex shapes. In general, the numerical models demonstrated a good ability to reproduce the results of the column tests accurately (Fig. 3 and Fig. S7), and high values of the determination coefficients were found (Table 2 and Table S6).

The sigmoidal deposition profiles of X_nZVI and N_nZVI were fitted accurately using a combination of blocking and linear interaction mechanisms. The need for a double retention mechanism to properly fit the retention profiles suggests the presence of a heterogenous particle population likely composed of large aggregates, for which sedimentation dominate the deposition process (modeled with the linear interaction mechanism), and smaller aggregates that instead exhibit electrostatic repulsive forces (modeled with the blocking site) driven by their not negligible surface charge (zeta potentials between 1 and -22 mV). For X_nZVI, the best-fit k_a values were 0.012–0.048 s^{-1} for the blocking site and 0.001–0.012 s^{-1} for the linear site. Similar k_a values were obtained for N_nZVI (0.009–0.032 and 0.001–0.003 s^{-1}, respectively). In addition, the maximum blocking concentration, S_{max}, was found to vary within similar ranges, indicating comparable migration properties of the two different crystalline phases (Table 2). Polyelectrolyte coatings have been confirmed to improve the mobility of nZVI in porous media (Jiemvarangkul et al., 2011; Lin et al., 2010; Raychoudhury et al., 2010). In the present study, the addition of an organic modifier changed the PA_nZVI deposition dynamics, which switched from the two-site model (blocking plus linear) employed for X_nZVI to a single-mechanism process. Specifically, a linear model was adopted to simulate the exponential profile of PA_nZVI, whereas a straining process was used to accurately fit the hyperexponential curve of PA_nZVI_com (Fig. 3). The occurrence of straining could be explained by the development of long-chain steric coatings on the surface of PA_nZVI_com, and to the presence of divalent and trivalent cations in the tap water used for the experiments. Indeed, when multivalent cations are present, bridging phenomena among the polymeric chains present on the surface of different particles can occur, thus leading to additional particle aggregation and consequent increase in the average particle size (Tiraferri et al., 2017; Tosco and Sethi, 2010). However, despite some accumulation of PA_nZVI_com observed at the column inlet, the values of the straining parameter β_{str} were much lower than the typical value of 0.432 proposed by Bradford et al. (2002) (Table 2). Such values show that straining was not dominant in the studied conditions, highlighting the linear transport behavior. These results agree with Bianco et al. (2023), who used a linear model to describe the transport of nZVI particles stabilized with a shear-thinning gel. The attachment rates for PA_nZVI and PA_nZVI_com were lower than those for X_nZVI at both the linear and blocking sites. This implies that organically modified nZVI may have better transport than unmodified X_nZVI. For Ox_nZVI, a dual-site model with blocking and straining mechanisms was used to describe the concentration profiles effectively. Also, in this case, the dual-site model suggests the presence of a heterogenous particle population in terms of aggregate size and surface charge. However, the β_{str} value revealed only a minimal effect of straining. Compared with X_nZVI, Ox_nZVI showed lower attachment rates, indicating enhanced mobility, although the S_{max} values were similar (Table 2). A dual-site blocking-linear model was used to fit the sigmoidal profiles of S_nZVI. Finally, a blocking and straining model was adopted for S_nZVI_com. The selection of the blocking site is consistent with the material's relatively high surface charge; however, the need to include a straining site to fit the retention profile suggests the presence of very large aggregates or the progressive growth of initial aggregates during transport within the column. All the other S_nZVI samples were properly fitted using a dual site model with a blocking and a linear retention site. Despite the same model being also used to fit X_nZVI data, lower kinetic coefficients were obtained for all sulfidated particles, suggesting better transport for this nZVI derivative. In particular, the blocking attachment rates were similar for all the S_nZVI samples and were one order of magnitude higher than those of the linear site (Table 2). The repulsive forces among S_nZVI particles, accentuated by their stronger negative surface charge (<−26 mV) compared to X_nZVI, significantly reduced their deposition. (Ko and Elimelech, 2000). Higher sulfidation levels in S-nZVI resulted in higher S_{max} values, demonstrating the lower mobility of the more sulfidated particles. A lower S_{max} typically enhances nZVI mobility due to faster saturation of deposition space (Li et al., 2015), aligning with slightly decreased zeta potential values as sulfidation increases.

Regarding real application of nZVI, we need to consider that we are dealing with injection of aggregates rather than nZVI single nanoparticles as evident from DLS measurement (Fig. S9). Aging experiments on X_nZVI and N_nZVI confirmed the stability of aggregates in time, showing no trend in aggregate size grown and stability of nZVI suspensions. Since magnetic attractive forces may dominate the mobility of nZVI, transport of microscale nZVI aggregates is rather dominated by Wan der Waals and electrostatic forces. Although magnetic forces can significantly influence the aggregation rate (Rosická and Šembera, 2013), their impact was not considered in this study because the suspension's stability was experimentally confirmed. Ultimately, the model's results aligned with the experimental data, supporting the hypothesis that the aggregate suspensions can be considered rather stable.

3.4. From radial simulations to real-world implementation

The modifications of X_nZVI were evaluated based on their ability to cover the greatest distance with the most effective spatial distribution at a sufficiently high concentration. Kinetic coefficients derived from the migration experimental results were employed to extrapolate nZVI transport to conditions resembling field scenarios, which were achieved by simulating the permeation injection of nZVI within a homogeneous

Table 2
Deposition mechanisms and range of transport parameters in column experiments.

	Blocking		Linear	Straining		Determination coefficient
	k_a	S_{max}	k_a	k_a	β_{str}	R^2
	($\times 10^{-3}$ s^{-1})	(g kg^{-1})	($\times 10^{-3}$ s^{-1})	($\times 10^{-3}$ s^{-1})	(−)	(%)
X_nZVI	11.9–47.7	4.0–17.9	1.0–12.4	–	–	98.8–99.6
N_nZVI	9.8–32.1	2.9–19.3	1.3–2.6	–	–	99.4–99.7
PA_nZVI	–	–	4.5–5.5	–	–	98.7–99.4
PA_nZVI_com	–	–	–	4.7–6.1	0.04–0.10	97.1–99.4
Ox_nZVI	6.3–9.8	4.0–15.2	–	3.4–3.8	0.07–0.10	99.1–99.2
S_nZVI_0.5	15.0–15.5	4.1–5.8	1.6–1.7	–	–	98.6–98.8
S_nZVI_1.0[a]	22.6	9.2	2.2	–	–	99.4
S_nZVI_2.0	14.5–29.4	5.1–15.2	1.8–2.4	–	–	99.6–99.8
S_nZVI_5.0	9.5–12.7	12.4–15.8	1.2–2.0	–	–	99.7–99.9
S_nZVI_com[a]	8.9	5.9	–	1.5	0.1	96.5

[a] only one experiment modeled.

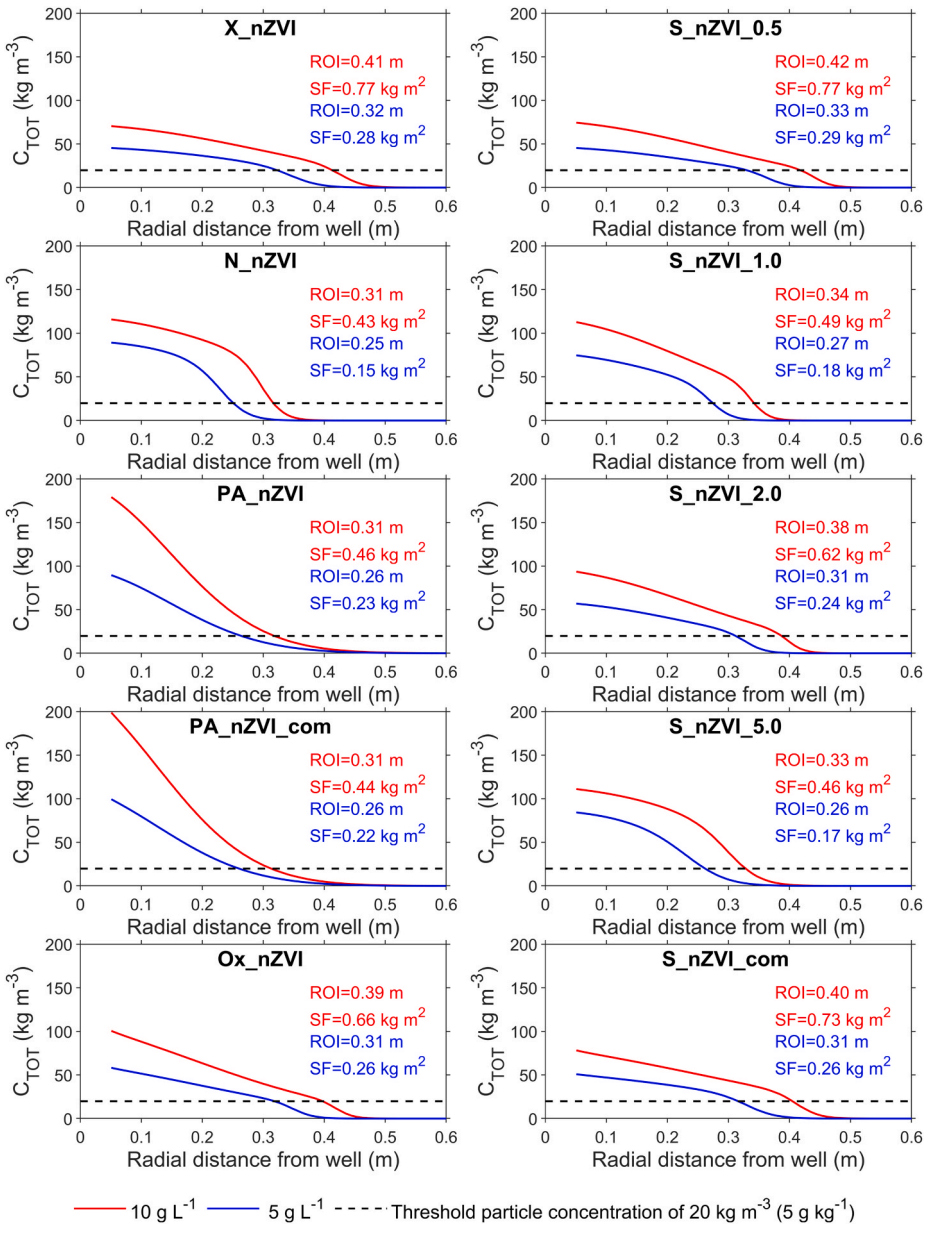

Fig. 4. Representative radial distribution of the X-nZVI and its derivatives at the end of the simulated scenarios. ROI and SF values for specific column experiments are depicted.

Table 3
Average ROI and SF values from radial injection simulations.

	ROI_{avg}		ROI_{avg}/ROI_{tracer}		SF_{avg}		SF_{avg}/SF_{tracer}	
	(m)		(%)		(kg m^2)		(%)	
Injection (g L^{-1})	5	10	5	10	5	10	5	10
X_nZVI	0.28	0.37	32	41	0.23	0.63	12	16
N_nZVI	0.27	0.35	31	39	0.21	0.54	11	14
PA_nZVI	0.26	0.32	30	36	0.25	0.51	13	13
PA_nZVI_com	0.26	0.33	30	37	0.29	0.59	15	15
Ox_nZVI	0.29	0.36	32	40	0.23	0.56	12	15
S_nZVI_0.5	0.32	0.40	36	45	0.27	0.72	14	19
S_nZVI_1.0	0.27	0.34	31	38	0.18	0.49	9	13
S_nZVI_2.0	0.29	0.36	33	40	0.21	0.56	11	14
S_nZVI_5.0	0.26	0.33	29	37	0.18	0.47	9	12
S_nZVI_com	0.31	0.40	35	45	0.26	0.73	14	19

radial domain (Tosco et al., 2018). A radial simulation was performed to predict the nZVI-specific concentration profile around the injection well using the $C_{a,i}$ values derived from the interpretation of the 1D experiments (Table S7, Fig. S10). Overall, the mobilities of the studied nZVI derivatives predicted by the radial simulations were consistent with the results observed in the column tests. However, field-scale simulations amplified the small differences among the tested nZVI that had already been observed at the laboratory scale. Significant variations were observed in the shape and magnitude of the simulated concentration profiles, which were influenced by the type of nZVI particles and their concentration in the injected suspension. Higher concentrations in the suspension directly resulted in elevated concentration profiles in the aquifer owing to the greater total mass of nZVI injected (Fig. 4). This trend was coherently mirrored by the behavior of the expected ROI, which varied between 0.26 and 0.32 m for the 5 g L^{-1} suspension and extended from 0.32 to 0.40 m for the 10 g L^{-1} injection scenarios (Table 3). However, when comparing various nZVI derivatives, the differences in ROI were rather small, showing an 8 cm range between the highest and lowest values at the same injected concentration. This is the reason why SF was proposed as an integrative measure to discern the differences more clearly in transport properties.

In terms of the nZVI dispersion around the center of the well, the shape of the concentration profiles mainly depended on the interaction between nZVI and the porous medium, which varied for each nZVI type. For instance, materials whose transport and deposition were primarily influenced by physical processes, such as straining (e.g., polyacrylic acid stabilized particles and oxide-passivated nZVI), exhibited exponentially decreasing concentration profiles with significant particle accumulation near the injection well. In contrast, when blocking was the dominant deposition mechanism (e.g., sulfidated nZVI), a more uniform distribution around the well, resulting in an almost flat profile, was predicted. The iron content, however, had only a minimal effect on the shape of the concentration profiles according to the model. The uniform distribution of nZVI reduced the need for the injection of large quantities. The need to define the spatial extent to which nZVI can operate effectively results from the fact that nZVI moves as a distinct mass, driven more by buoyancy than by diffusion or dispersion, such as dissolved substances (Viotti et al., 2022). In this study, a quantitative measurement of the uniformity of nZVI distribution near the injection point was introduced through SF. Considering the 10 g L^{-1} scenario, the SF, which describes the steepness of the concentration curve, ranged between 47 kg m^2 for sharp profiles with particle accumulation near the injection point and 73 kg m^2 for simulations where a more homogeneous nZVI distribution was achieved. Comparison of the ROI and SF values across the nZVI derivatives was only valid at identical injection concentrations and did not yield a clear ranking based on nZVI migration effectiveness. To quantify the transport behavior of the nZVI derivatives at two different concentrations, the ROI and SF values were normalized by dividing them by the values of a tracer that did not interact with the porous media (Fig. 5). A slightly more homogeneous spatial distribution was expected for X_nZVI than for N_nZVI, as demonstrated by the higher shape factor value (Table 3). The distinctively sharp concentration profiles of PA_nZVI and PA_nZVI_com, together with Ox_nZVI, resulted in a notable retention of nZVI close to the injection point, as emphasized by having some of the lowest estimated SF values at a concentration of 10 g L^{-1} (Fig. 4, Table S7). In contrast, S_nZVI_0.5 and S_nZVI_com, with the most uniform concentration profiles across distances, also had the highest SF values. In particular, the 0.5% sulfidation (S_nZVI_0.5) led to an increase of around 10% of the ROI and of 14% of the SF compared to the unmodified X_nZVI. A similar mobility improvement was also observed for the commercial S_nZVI_com. In contrast, nZVI with higher levels of sulfidation showed no improvement or even a decline in ROI and SF. Specifically, the S_nZVI_5.0 particles exhibited the poorest transport behavior, with an 11% reduction in ROI and a 25% decrease in SF compared to the unmodified X_nZVI. Therefore, the combination of a low degree of sulfidation and organic modification could bring about the desired effect of achieving very good radial and vertical iron distribution in the subsurface.

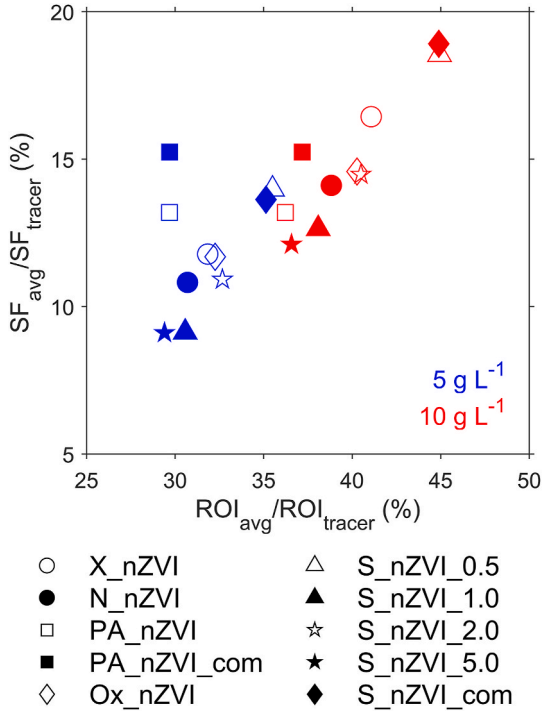

Fig. 5. Normalization of ROI and SF against non-interacting tracer for enhanced comparability of X_nZVI and its derivatives transport.

4. Conclusions

This research provides a comprehensive comparison of various nZVI derivatives under controlled conditions, focusing on their migration mechanisms and potential applications in environmental remediation. By optimizing transport monitoring techniques, we successfully aligned experimental results with mathematical models, creating a robust framework for predicting and controlling the transport of nitrided, organically modified, oxide-passivated, and sulfidated nZVI derivatives. Radial simulations using the MNMs numerical code enabled predictions of the radius of influence (ROI) and particle distribution homogeneity (SF) around the well in field-scale injections.

The study experimentally confirmed two main properties of nZVI derivatives that significantly impact mobility: magnetic nature and surface charge. Magnetic attraction led to rapid aggregation and sedimentation of large nZVI aggregates, while the negative surface charge from sulfides, oxides, or organic compounds introduced electrostatic repulsion in smaller aggregates, enhancing their mobility in porous media. This dual behavior required modeling with a double retention mechanism: large aggregates, influenced by sedimentation, were modeled using a linear or straining interaction mechanism, while smaller aggregates, exhibiting repulsive forces, were modeled using a blocking mechanism. The migration of X_nZVI and N_nZVI was comparable, but the results suggest that surface modification with organic compounds like polyacrylic acid could enhance mobility and performance of N_nZVI particles. Findings of this study allowed to compare the expected mobility behavior of different nZVI derivatives in sandy aquifers. Moreover, the model proved to be a flexible tool to extrapolate and generalize results to field scale conditions and support the design of real nZVI injections. Overall, the study highlights the importance of selecting appropriate surface modifications to achieve optimal nZVI performance in environmental remediation. The results indicate that sulfidation and organic modifications, such as those applied to S_nZVI

and PA_nZVI, improve mobility while also ensuring controlled particle retention in target areas, which is crucial for effective in-situ remediation. By balancing reactivity, mobility and retention, nZVI derivatives can be tailored for more effective and controlled remediation outcomes, contributing to their commercial viability in environmental clean-up efforts.

Funding

The work was supported from ERDF/ESF project TECHSCALE (No. CZ.02.01.01/00/22_008/0004587). This study was also carried out within the Ministerial Decree No. 1062/2021 and received funding from the FSE REACT-EU - PON Ricerca e Innovazione 2014–2020.

CRediT authorship contribution statement

Veronika Veselská: Writing – review & editing, Writing – original draft, Visualization, Supervision, Resources, Project administration, Investigation, Conceptualization. **Leonardo Magherini:** Writing – review & editing, Visualization, Validation, Software, Methodology, Investigation. **Carlo Bianco:** Writing – review & editing, Methodology, Investigation, Formal analysis, Data curation, Conceptualization. **Jan Šembera:** Writing – review & editing, Software, Methodology, Formal analysis, Data curation. **Petr Parma:** Validation, Methodology, Investigation. **Viktorie Víchová:** Visualization, Investigation, Data curation. **Rajandrea Sethi:** Writing – review & editing, Funding acquisition. **Jan Filip:** Writing – review & editing, Funding acquisition.

Declaration of generative AI and AI-assisted technologies in the writing process

During the preparation of this work the authors used ChatGPT 4 to improve language and readability of the manuscript. After using this tool, the authors reviewed and edited the content as needed and take full responsibility for the content of the publication.

Declaration of competing interest

The authors declare that they have no known competing financial interests or personal relationships that could have appeared to influence the work reported in this paper.

Data availability

The data supporting this study are available in the ZENODO repository.

Acknowledgements

We thank Ivo Medřík, Erik Mikeska for material synthesis, transport, and preparation for migration experiments, Jana Stráská for TEM measurements, Jiří Hošek for SEM/EDX, Martin Petr for XPS measurements, and Josef Kašlík and Gildas Ratié for consultations. This manuscript reflects only the authors' views and opinions, neither the European Union nor the European Commission can be considered responsible for them. The English language of the manuscript has been corrected by the Elsevier English Editing Service. The authors thank the editor and seven anonymous reviewers for their constructive comments and suggestions.

Appendix A. Supplementary data

Supplementary data to this article can be found online at https://doi.org/10.1016/j.jenvman.2024.122552.

References

Ahmad, M.A., Adeel, M., Shakoor, N., Javed, R., Ishfaq, M., Peng, Y., Zain, M., Azeem, I., Ali, I., Usman, M., Wu, Z., Gohari, G., Xu, M., Rui, Y., Zhang, Z., White, J.C., Deng, X., 2023. Modifying engineered nanomaterials to produce next generation agents for environmental remediation. Sci. Total Environ. 894, 164861. https://doi.org/10.1016/j.scitotenv.2023.164861.

Al-Hashimi, O., Hashim, K., Loffill, E., Marolt Čebašek, T., Nakouti, I., Faisal, A.A.H., Al-Ansari, N., 2021. A comprehensive review for groundwater contamination and remediation: occurrence, migration and adsorption modelling. Molecules 26, 5913. https://doi.org/10.3390/molecules26195913.

Bhattacharjee, S., Ghoshal, S., 2018. Optimal design of sulfidated nanoscale zerovalent iron for enhanced trichloroethene degradation. Environ. Sci. Technol. 52, 11078–11086. https://doi.org/10.1021/acs.est.8b02399.

Bianco, C., Mondino, F., Casasso, A., 2023. Improved delivery of nanoscale zero-valent iron particles and simplified design tools for effective aquifer nanoremediation. Water 15, 2303. https://doi.org/10.3390/w15122303.

Bianco, C., Patiño Higuita, J.E., Tosco, T., Tiraferri, A., Sethi, R., 2017. Controlled deposition of particles in porous media for effective aquifer nanoremediation. Sci. Rep. 7, 12992. https://doi.org/10.1038/s41598-017-13423-y.

Bianco, C., Tosco, T., Sethi, R., 2016. A 3-dimensional micro- and nanoparticle transport and filtration model (MNM3D) applied to the migration of carbon-based nanomaterials in porous media. J. Contam. Hydrol. 193, 10–20. https://doi.org/10.1016/j.jconhyd.2016.08.006.

Boccardo, G., Tosco, T., Fujisaki, A., Messina, F., Raoof, A., Aguilera, D.R., Crevacore, E., Marchisio, D.L., Sethi, R., 2020. A review of transport of nanoparticles in porous media. In: Nanomaterials for the Detection and Removal of Wastewater Pollutants. Elsevier, pp. 351–381. https://doi.org/10.1016/B978-0-12-818489-9.00013-X.

Bradford, S.A., Torkzaban, S., 2008. Colloid transport and retention in unsaturated porous media: a review of interface-, collector-, and pore-scale processes and models. Vadose Zone J. 7, 667–681. https://doi.org/10.2136/vzj2007.0092.

Bradford, S.A., Yates, S.R., Bettahar, M., Simunek, J., 2002. Physical factors affecting the transport and fate of colloids in saturated porous media. Water Resour. Res. 38. https://doi.org/10.1029/2002WR001340, 63-1-63–12.

Brumovský, M., Filip, J., Malina, O., Oborná, J., Sracek, O., Reichenauer, T.G., Andrýsková, P., Zbořil, R., 2020. Core–shell Fe/FeS nanoparticles with controlled shell thickness for enhanced trichloroethylene removal. ACS Appl. Mater. Interfaces 12, 35424–35434. https://doi.org/10.1021/acsami.0c08626.

Brumovský, M., Micić, V., Oborná, J., Filip, J., Hofmann, T., Tunega, D., 2023. Iron nitride nanoparticles for rapid dechlorination of mixed chlorinated ethene contamination. J. Hazard Mater. 442, 129988. https://doi.org/10.1016/j.jhazmat.2022.129988.

Brumovský, M., Oborná, J., Lacina, P., Hegedüs, M., Sracek, O., Kolařík, J., Petr, M., Kašlík, J., Hofmann, T., Filip, J., 2021. Sulfidated nano-scale zerovalent iron is able to effectively reduce in situ hexavalent chromium in a contaminated aquifer. J. Hazard Mater. 405, 124665. https://doi.org/10.1016/j.jhazmat.2020.124665.

Brumovský, M., Oborná, J., Micić, V., Malina, O., Kašlík, J., Tunega, D., Kolos, M., Hofmann, T., Karlický, F., Filip, J., 2022. Iron nitride nanoparticles for enhanced reductive dechlorination of trichloroethylene. Environ. Sci. Technol. https://doi.org/10.1021/acs.est.1c08282.

Černík, M., Nosek, J., Filip, J., Hrabal, J., Elliott, D.W., Zbořil, R., 2019. Electric-field enhanced reactivity and migration of iron nanoparticles with implications for groundwater treatment technologies: proof of concept. Water Res. 154, 361–369. https://doi.org/10.1016/j.watres.2019.01.058.

Chen, B., Lv, N., Xu, W., Gong, L., Sun, T., Liang, L., Gao, B., He, F., 2023. Transport of nanoscale zero-valent iron in saturated porous media: effects of grain size, surface metal oxides, and sulfidation. Chemosphere 313, 137512. https://doi.org/10.1016/j.chemosphere.2022.137512.

Cheng, Y., Dong, H., Hao, T., 2021. CaCO3 coated nanoscale zero-valent iron (nZVI) for the removal of chromium(VI) in aqueous solution. Separ. Purif. Technol. 257, 117967. https://doi.org/10.1016/j.seppur.2020.117967.

Cheng, Y., Hu, P., Hao, T., 2024. Elucidating the impact of sulfur precursors on the reactivity, toxicity, and colloidal stability of post-sulfidized nanoscale zerovalent iron. Separ. Purif. Technol. 328, 125132. https://doi.org/10.1016/j.seppur.2023.125132.

Dhanush Raj, A., Ahammed, M.M., 2024. Chapter 22 - nano-zerovalent iron for water and wastewater treatment. In: Kumar Kailasa, S., Park, T.J., Singhal, R.K. (Eds.), Nanomaterials in Environmental Analysis. Elsevier, pp. 505–536. https://doi.org/10.1016/B978-0-12-820643-0.00025-0.

Dong, H., Lo, I.M.C., 2014. Transport of surface-modified nano zero-valent iron (SM-NZVI) in saturated porous media: effects of surface stabilizer type, subsurface geochemistry, and contaminant loading. Water Air Soil Pollut. 225, 2107. https://doi.org/10.1007/s11270-014-2107-6.

Eljamal, R., Eljamal, O., Maamoun, I., Yilmaz, G., Sugihara, Y., 2020. Enhancing the characteristics and reactivity of nZVI: polymers effect and mechanisms. J. Mol. Liq. 315, 113714. https://doi.org/10.1016/j.molliq.2020.113714.

Fan, D., Lan, Y., Tratnyek, P.G., Johnson, R.L., Filip, J., O'Carroll, D.M., Nunez Garcia, A., Agrawal, A., 2017. Sulfidation of iron-based materials: a review of processes and implications for water treatment and remediation. Environ. Sci. Technol. 51, 13070–13085. https://doi.org/10.1021/acs.est.7b04177.

Fan, D., O'Brien Johnson, G., Tratnyek, P.G., Johnson, R.L., 2016. Sulfidation of nano zerovalent iron (nZVI) for improved selectivity during in-situ chemical reduction (ISCR). Environ. Sci. Technol. 50, 9558–9565. https://doi.org/10.1021/acs.est.6b02170.

Fazeli Sangani, M., Owens, G., Fotovat, A., 2019. Transport of engineered nanoparticles in soils and aquifers. Environ. Rev. 27, 43–70. https://doi.org/10.1139/er-2018-0022.

Filip, J., Karlický, F., Marušák, Z., Lazar, P., Černík, M., Otyepka, M., Zbořil, R., 2014. Anaerobic reaction of nanoscale zerovalent iron with water: mechanism and kinetics. J. Phys. Chem. C 118, 13817–13825. https://doi.org/10.1021/jp501846f.

Galdames, A., Ruiz-Rubio, L., Orueta, M., Sánchez-Arzalluz, M., Vilas-Vilela, J.L., 2020. Zero-valent iron nanoparticles for soil and groundwater remediation. Int. J. Environ. Res. Publ. Health 17, 5817. https://doi.org/10.3390/ijerph17165817.

Gao, F., Zhang, M., Li, S., Liu, L., Tang, J., 2024. Effect of physical and chemical co-application of biochar and sulfidated nano scale zero valent iron on the NB degradation in soil: key roles of biochar. Separ. Purif. Technol. 353, 128546. https://doi.org/10.1016/j.seppur.2024.128546.

Garcia, A.N., Zhang, Y., Ghoshal, S., He, F., O'Carroll, D.M., 2021. Recent advances in sulfidated zerovalent iron for contaminant transformation. Environ. Sci. Technol. 55, 8464–8483. https://doi.org/10.1021/acs.est.1c01251.

Han, Y., Yan, W., 2016. Reductive dechlorination of trichloroethene by zero-valent iron nanoparticles: reactivity enhancement through sulfidation treatment. Environ. Sci. Technol. 50, 12992–13001. https://doi.org/10.1021/acs.est.6b03997.

He, S., Zhu, F., Li, L., Ren, W., 2018. Box–Behnken design for the optimization of the removal of Cr(VI) in soil leachate using nZVI/Ni bimetallic particles. Soil Sediment Contam.: Int. J. 27, 658–673. https://doi.org/10.1080/15320383.2018.1502744.

Jia, Z., Shu, Y., Huang, R., Liu, J., Liu, L., 2018. Enhanced reactivity of nZVI embedded into supermacroporous cryogels for highly efficient Cr(VI) and total Cr removal from aqueous solution. Chemosphere 199, 232–242. https://doi.org/10.1016/j.chemosphere.2018.02.021.

Jiemvarangkul, P., Zhang, W., Lien, H.-L., 2011. Enhanced transport of polyelectrolyte stabilized nanoscale zero-valent iron (nZVI) in porous media. Chemical Engineering Journal, Environmental Nanotechnology 170, 482–491. https://doi.org/10.1016/j.cej.2011.02.065.

Karn, B., Kuiken, T., Otto, M., 2009. Nanotechnology and in situ remediation: a review of the benefits and potential risks. Environ. Health Perspect. 117, 1813–1831. https://doi.org/10.1289/ehp.0900793.

Kašlík, J., Kolařík, J., Filip, J., Medřík, I., Tomanec, O., Petr, M., Malina, O., Zbořil, R., Tratnyek, P.G., 2018. Nanoarchitecture of advanced core-shell zero-valent iron particles with controlled reactivity for contaminant removal. Chem. Eng. J. 354, 335–345. https://doi.org/10.1016/j.cej.2018.08.015.

Keochanh, D., Tongkamnoi, S., Phenrat, T., 2024. Can polymeric surface modification and sulfidation of nanoscale zerovalent iron (NZVI) improve arsenic-contaminated agricultural soil restoration via ex situ magnet-assisted soil washing? Environ. Chem. 20, 302–318. https://doi.org/10.1071/EN23078.

Klimkova, S., Cernik, M., Lacinova, L., Filip, J., Jancik, D., Zboril, R., 2011. Zero-valent iron nanoparticles in treatment of acid mine water from in situ uranium leaching. Chemosphere 82, 1178–1184. https://doi.org/10.1016/j.chemosphere.2010.11.075.

Ko, C.-H., Bhattacharjee, S., Elimelech, M., 2000. Coupled influence of colloidal and hydrodynamic interactions on the RSA dynamic blocking function for particle deposition onto packed spherical collectors. J. Colloid Interface Sci. 229, 554–567. https://doi.org/10.1006/jcis.2000.7062.

Ko, C.-H., Elimelech, M., 2000. The "shadow effect" in colloid transport and deposition dynamics in granular porous media: measurements and mechanisms. Environ. Sci. Technol. 34, 3681–3689.

Kocur, C.M., O'Carroll, D.M., Sleep, B.E., 2013. Impact of nZVI stability on mobility in porous media. J. Contam. Hydrol. 145, 17–25. https://doi.org/10.1016/j.jconhyd.2012.11.001.

Kuyukina, M.S., Makarova, M.V., Pistsova, O.N., Glebov, G.G., Osipenko, M.A., Ivshina, I. B., 2022. Exposure to metal nanoparticles changes zeta potentials of Rhodococcus cells. Heliyon 8, e11632. https://doi.org/10.1016/j.heliyon.2022.e11632.

Lacina, P., Dvorak, V., Vodickova, E., Barson, P., Kalivoda, J., Goold, S., 2015. The application of nano-sized zero-valent iron for in situ remediation of chlorinated ethylenes in groundwater: a field case study. Water Environ. Res. 87, 326–333.

Lang, Y., Yu, Y., Zou, H., Ye, J., Zhang, S., 2022. Performance and mechanisms of sulfidated nanoscale zero-valent iron materials for toxic TCE removal from the groundwater. Int J Environ Res Public Health 19, 6299. https://doi.org/10.3390/ijerph19106299.

Latif, A., Sheng, D., Sun, K., Si, Y., Azeem, M., Abbas, A., Bilal, M., 2020. Remediation of heavy metals polluted environment using Fe-based nanoparticles: mechanisms, influencing factors, and environmental implications. Environ. Pollut. 264, 114728. https://doi.org/10.1016/j.envpol.2020.114728.

Li, H., Zhao, Y.-S., Han, Z.-T., Hong, M., 2015. Transport of sucrose-modified nanoscale zero-valent iron in saturated porous media: role of media size, injection rate and input concentration. Water Sci. Technol. 72, 1463–1471. https://doi.org/10.2166/wst.2015.308.

Li, S., Wang, W., Liu, Y., Zhang, W., 2014. Zero-valent iron nanoparticles (nZVI) for the treatment of smelting wastewater: a pilot-scale demonstration. Chem. Eng. J. 254, 115–123. https://doi.org/10.1016/j.cej.2014.05.111.

Li, Y., Wang, Y., Pennell, K.D., Abriola, L.M., 2008. Investigation of the transport and deposition of fullerene (C60) nanoparticles in quartz sands under varying flow conditions. Environ. Sci. Technol. 42, 7174–7180. https://doi.org/10.1021/es801305y.

Lin, Y.-H., Tseng, H.-H., Wey, M.-Y., Lin, M.-D., 2010. Characteristics of two types of stabilized nano zero-valent iron and transport in porous media. Sci. Total Environ. 408, 2260–2267. https://doi.org/10.1016/j.scitotenv.2010.01.039.

Ling, X., Yan, Z., Liu, Y., Lu, G., 2021. Transport of nanoparticles in porous media and its effects on the co-existing pollutants. Environ Pollut 283, 117098. https://doi.org/10.1016/j.envpol.2021.117098.

Liu, J., Liu, A., Guo, J., Zhou, T., Zhang, W., 2021. Enhanced aggregation and sedimentation of nanoscale zero-valent iron (nZVI) with polyacrylamide modification. Chemosphere 263, 127875. https://doi.org/10.1016/j.chemosphere.2020.127875.

Liu, M., Chen, G., Xu, L., He, Z., Ye, Y., 2024. Environmental remediation approaches by nanoscale zero valent iron (nZVI) based on its reductivity: a review. RSC Adv. 14, 21118–21138. https://doi.org/10.1039/D4RA02789B.

Liu, Y., Zhang, Y., Lan, S., Hou, S., 2019. Migration experiment and numerical simulation of modified nanoscale zero-valent iron (nZVI) in porous media. J. Hydrol. 579, 124193. https://doi.org/10.1016/j.jhydrol.2019.124193.

Mackenzie, K., Georgi, A., 2019. NZVI synthesis and characterization. In: Phenrat, T., Lowry, G.V. (Eds.), Nanoscale Zerovalent Iron Particles for Environmental Restoration: from Fundamental Science to Field Scale Engineering Applications. Springer International Publishing, Cham, pp. 45–95. https://doi.org/10.1007/978-3-319-95340-3_2.

Molnar, I.L., Sanematsu, P.C., Gerhard, J.I., Willson, C.S., O'Carroll, D.M., 2016. Quantified pore-scale nanoparticle transport in porous media and the implications for colloid filtration theory. Langmuir 32. https://doi.org/10.1021/acs.langmuir.6b01233.

Mondino, F., Piscitello, A., Bianco, C., Gallo, A., de Folly D'Auris, A., Tosco, T., Tagliabue, M., Sethi, R., 2020. Injection of zerovalent iron gels for aquifer nanoremediation: lab experiments and modeling. Water 12, 826. https://doi.org/10.3390/w12030826.

Němeček, J., Pokorný, P., Lhotský, O., Knytl, V., Najmanová, P., Steinová, J., Černík, M., Filipová, A., Filip, J., Cajthaml, T., 2016. Combined nano-biotechnology for in-situ remediation of mixed contamination of groundwater by hexavalent chromium and chlorinated solvents. Sci. Total Environ. 563–564, 822–834. https://doi.org/10.1016/j.scitotenv.2016.01.019.

Ng, W.M., Lim, J.K., 2022. Complex interplay between colloidal stability, transport, chemical reactivity and magnetic separability of polyelectrolyte-functionalized nanoscale zero-valent iron particles (nZVI) toward their environmental engineering application. Colloid and Interface Science Communications 46, 100582. https://doi.org/10.1016/j.colcom.2021.100582.

Nune, S.K., Miller, Q.R.S., Schaef, H.T., Jian, T., Song, M., Li, D., Shuttanandan, V., McGrail, B.P., 2022. Transport of polymer-coated metal–organic framework nanoparticles in porous media. Sci. Rep. 12, 13962. https://doi.org/10.1038/s41598-022-18264-y.

Nunez Garcia, A., Boparai, H.K., Chowdhury, A.I.A., de Boer, C.V., Kocur, C.M.D., Passeport, E., Sherwood Lollar, B., Austrins, L.M., Herrera, J., O'Carroll, D.M., 2020a. Sulfidated nano zerovalent iron (S-nZVI) for in situ treatment of chlorinated solvents: a field study. Water Res. 174, 115594. https://doi.org/10.1016/j.watres.2020.115594.

Nunez Garcia, A., Boparai, H.K., de Boer, C.V., Chowdhury, A.I.A., Kocur, C.M.D., Austrins, L.M., Herrera, J., O'Carroll, D.M., 2020b. Fate and transport of sulfidated nano zerovalent iron (S-nZVI): a field study. Water Res. 170, 115319. https://doi.org/10.1016/j.watres.2019.115319.

O'Carroll, D., Sleep, B., Krol, M., Boparai, H., Kocur, C., 2013. Nanoscale zero valent iron and bimetallic particles for contaminated site remediation. Advances in Water Resources, 35th Year Anniversary Issue 51, 104–122. https://doi.org/10.1016/j.advwatres.2012.02.005.

Parma, P., Ševců, A., Černík, M., 2020. Tool I: characterization of nZVI mobility in 1D and cascade columns by ferromagnetic susceptibility sensor. In: Filip, J., Cajthaml, T., Najmanová, P., Černík, M., Zbořil, R. (Eds.), Advanced Nano-Bio Technologies for Water and Soil Treatment, Applied Environmental Science and Engineering for a Sustainable Future. Springer International Publishing, Cham, pp. 609–617. https://doi.org/10.1007/978-3-030-29840-1_30.

Pasinszki, T., Krebsz, M., 2020. Synthesis and application of zero-valent iron nanoparticles in water treatment, environmental remediation, catalysis, and their biological effects. Nanomaterials 10, 917. https://doi.org/10.3390/nano10050917.

Pelley, A.J., Tufenkji, N., 2008. Effect of particle size and natural organic matter on the migration of nano- and microscale latex particles in saturated porous media. J. Colloid Interface Sci. 321, 74–83. https://doi.org/10.1016/j.jcis.2008.01.046.

Plessl, K., Russ, A., Vollprecht, D., 2023. Application and development of zero-valent iron (ZVI) for groundwater and wastewater treatment. Int. J. Environ. Sci. Technol. 20, 6913–6928. https://doi.org/10.1007/s13762-022-04536-7.

Pulido-Reyes, G., Magherini, L., Bianco, C., Sethi, R., von Gunten, U., Kaegi, R., Mitrano, D.M., 2022. Nanoplastics removal during drinking water treatment: laboratory- and pilot-scale experiments and modeling. J. Hazard Mater. 436, 129011. https://doi.org/10.1016/j.jhazmat.2022.129011.

Raychoudhury, T., Naja, G., Ghoshal, S., 2010. Assessment of transport of two polyelectrolyte-stabilized zero-valent iron nanoparticles in porous media. Journal of Contaminant Hydrology. Manufactured Nanomaterials in Subsurface Systems 118, 143–151. https://doi.org/10.1016/j.jconhyd.2010.09.005.

Raychoudhury, T., Tufenkji, N., Ghoshal, S., 2014. Straining of polyelectrolyte-stabilized nanoscale zero valent iron particles during transport through granular porous media. Water Res. 50, 80–89. https://doi.org/10.1016/j.watres.2013.11.038.

Ribas, D., Černík, M., Benito, J.A., Filip, J., Marti, V., 2017. Activation process of air stable nanoscale zero-valent iron particles. Chem. Eng. J. 320, 290–299. https://doi.org/10.1016/j.cej.2017.03.056.

Rosická, D., Šembera, J., 2013. Changes in the nanoparticle aggregation rate due to the additional effect of electrostatic and magnetic forces on mass transport coefficients. Nanoscale Res. Lett. 8, 20. https://doi.org/10.1186/1556-276X-8-20.

Rosická, D., Sembera, J., 2011. Influence of structure of iron nanoparticles in aggregates on their magnetic properties. Nanoscale Res. Lett. 6, 527. https://doi.org/10.1186/1556-276X-6-527.

Saleh, N., Kim, H.-J., Phenrat, T., Matyjaszewski, K., Tilton, R.D., Lowry, G.V., 2008. Ionic strength and composition affect the mobility of surface-modified Fe0 nanoparticles in water-saturated sand columns. Environ. Sci. Technol. 42, 3349–3355. https://doi.org/10.1021/es071936b.

Semerád, J., Filip, J., Ševců, A., Brumovský, M., Nguyen, N.H.A., Mikšíček, J., Lederer, T., Filipová, A., Boháčková, J., Cajthaml, T., 2020. Environmental fate of sulfidated nZVI particles: the interplay of nanoparticle corrosion and toxicity during aging. Environ. Sci.: Nano 7, 1794–1806. https://doi.org/10.1039/D0EN00075B.

Semerád, J., Ševců, A., Nguyen, N.H.A., Hrabák, P., Špánek, R., Bobčíková, K., Pospíšková, K., Filip, J., Medřík, I., Kaslík, J., Šafařík, I., Filipová, A., Nosek, J., Pivokonský, M., Cajthaml, T., 2021. Discovering the potential of an nZVI-biochar composite as a material for the nanobioremediation of chlorinated solvents in groundwater: degradation efficiency and effect on resident microorganisms. Chemosphere 281, 130915. https://doi.org/10.1016/j.chemosphere.2021.130915.

Sethi, R., Molfetta, A.D., 2019. Groundwater Engineering: A Technical Approach to Hydrogeology, Contaminant Transport and Groundwater Remediation. Springer.

Seymour, M.B., Chen, G., Su, C., Li, Y., 2013. Transport and retention of colloids in porous media: does shape really matter? Environ. Sci. Technol. 47, 8391–8398. https://doi.org/10.1021/es4016124.

Shan, A., Idrees, A., Zaman, W.Q., Abbas, Z., Ali, M., Rehman, M.S.U., Hussain, S., Danish, M., Gu, X., Lyu, S., 2021. Synthesis of nZVI-Ni@BC composite as a stable catalyst to activate persulfate: trichloroethylene degradation and insight mechanism. J. Environ. Chem. Eng. 9, 104808. https://doi.org/10.1016/j.jece.2020.104808.

Shen, J., Chen, H., Xu, N., Liu, Y., Sun, W., Ma, X., Sun, R., Gao, Y., Zhao, J., 2024. Molybdate modified nano zero-valent iron via green synthesis enhances Cr(VI) reduction during their cotransport in water-saturated porous media. Chem. Eng. J. 479, 147599. https://doi.org/10.1016/j.cej.2023.147599.

Skácelová, P., Lebed, P., Filip, J., Oughton, D., Zbořil, R., 2020. Tracing of iron nanoparticles using an elemental signatures approach: laboratory and field-scale verification. Environ. Sci.: Nano 7, 623–633. https://doi.org/10.1039/C9EN00799G.

Song, I.-G., Kang, Y.-G., Kim, J.-H., Yoon, H., Um, W.Y., Chang, Y.-S., 2023. Assessment of sulfidated nanoscale zerovalent iron for *in-situ* remediation of cadmium-contaminated acidic groundwater at a zinc smelter. J. Hazard Mater. 441, 129915. https://doi.org/10.1016/j.jhazmat.2022.129915.

Soukupova, J., Zboril, R., Medrik, I., Filip, J., Safarova, K., Ledl, R., Mashlan, M., Nosek, J., Cernik, M., 2015. Highly concentrated, reactive and stable dispersion of zero-valent iron nanoparticles: direct surface modification and site application. Chem. Eng. J. 262, 813–822. https://doi.org/10.1016/j.cej.2014.10.024.

Stejskal, V., Lederer, T., Kvapil, P., Slunsky, J., Skácelová, P., 2017. NanoRem pilot site – spolchemie I, Czech republic: nanoscale zero-valent iron remediation of chlorinated hydrocarbons. NanoRem bulletin 2017, 1–8.

Su, Y., Jassby, D., Zhang, Y., Keller, A.A., Adeleye, A.S., 2020. Comparison of the colloidal stability, mobility, and performance of nanoscale zerovalent iron and sulfidated derivatives. J. Hazard Mater. 396, 122691. https://doi.org/10.1016/j.jhazmat.2020.122691.

Su, Y., Lowry, G.V., Jassby, D., Zhang, Y., 2019. Sulfide-modified NZVI (S-nzvi): synthesis, characterization, and reactivity. In: Phenrat, T., Lowry, G.V. (Eds.), Nanoscale Zerovalent Iron Particles for Environmental Restoration: from Fundamental Science to Field Scale Engineering Applications. Springer International Publishing, Cham, pp. 359–386. https://doi.org/10.1007/978-3-319-95340-3_9.

Tian, H., Liang, Y., Yang, D., Sun, Y., 2020. Characteristics of PVP–stabilised NZVI and application to dechlorination of soil–sorbed TCE with ionic surfactant. Chemosphere 239, 124807. https://doi.org/10.1016/j.chemosphere.2019.124807.

Ting, H.Z., Bedrikovetsky, P., Tian, Z.F., Carageorgos, T., 2021. Impact of shape on particle detachment in linear shear flows. Chem. Eng. Sci. 241, 116658. https://doi.org/10.1016/j.ces.2021.116658.

Tiraferri, A., Saldarriaga Hernandez, L.A., Bianco, C., Tosco, T., Sethi, R., 2017. Colloidal behavior of goethite nanoparticles modified with humic acid and implications for aquifer reclamation. J. Nanoparticle Res. 19, 107. https://doi.org/10.1007/s11051-017-3814-x.

Tosco, T., Bianco, C., Sethi, R., 2018. An integrated experimental and modeling approach to assess the mobility of iron-based nanoparticles in groundwater systems. In: Iron Nanomaterials for Water and Soil Treatment. Jenny Stanford Publishing.

Tosco, T., Petrangeli Papini, M., Cruz Viggi, C., Sethi, R., 2014a. Nanoscale zerovalent iron particles for groundwater remediation: a review. Journal of Cleaner Production, Emerging industrial processes for water management 77, 10–21. https://doi.org/10.1016/j.jclepro.2013.12.026.

Tosco, T., Gastone, F., Sethi, R., 2014b. Guar gum solutions for improved delivery of iron particles in porous media (Part 2): iron transport tests and modeling in radial geometry. J. Contam. Hydrol. 166, 34–51. https://doi.org/10.1016/j.jconhyd.2014.06.014.

Tosco, T., Sethi, R., 2010. Transport of non-Newtonian suspensions of highly concentrated micro- and nanoscale iron particles in porous media: a modeling approach. Environ. Sci. Technol. 44, 9062–9068. https://doi.org/10.1021/es100868n.

Tosco, T., Sethi, R., 2009. MNM1D: a numerical code for colloid transport in porous media: implementation and validation. AJES 5, 517–525. https://doi.org/10.3844/ajessp.2009.517.525.

Tosco, T., Tiraferri, A., Sethi, R., 2009. Ionic strength dependent transport of microparticles in saturated porous media: modeling mobilization and immobilization phenomena under transient chemical conditions. Environ. Sci. Technol. 43, 4425–4431. https://doi.org/10.1021/es900245d.

Tufenkji, N., Elimelech, M., 2004. Correlation equation for predicting single-collector efficiency in physicochemical filtration in saturated porous media. Environ. Sci. Technol. 38, 529–536. https://doi.org/10.1021/es034049r.

Vecchia, E.D., Coisson, M., Appino, C., Vinai, F., Sethi, R., 2009a. Magnetic characterization and interaction modeling of zerovalent iron nanoparticles for the remediation of contaminated aquifers. J. Nanosci. Nanotechnol. 9, 3210–3218. https://doi.org/10.1166/jnn.2009.047.

Vecchia, E.D., Luna, M., Sethi, R., 2009b. Transport in porous media of highly concentrated iron micro- and nanoparticles in the presence of xanthan gum. Environ. Sci. Technol. 43, 8942–8947. https://doi.org/10.1021/es901897d.

Velimirovic, M., Bianco, C., Ferrantello, N., Tosco, T., Casasso, A., Sethi, R., Schmid, D., Wagner, S., Miyajima, K., Klaas, N., Meckenstock, R.U., von der Kammer, F., Hofmann, T., 2020. A large-scale 3D study on transport of humic acid-coated goethite nanoparticles for aquifer remediation. Water 12, 1207. https://doi.org/10.3390/w12041207.

Viotti, P., Sappa, G., Tatti, F., Andrei, F., 2022. nZVI mobility and transport: laboratory test and numerical model. Hydrology 9, 196. https://doi.org/10.3390/hydrology9110196.

Visentin, C., Braun, A.B., Reginatto, C., Cecchin, I., Vanzetto, G.V., Thomé, A., 2024. Are contaminated soil and groundwater remediation with nanoscale zero-valent iron sustainable? An analysis of case studies. Environ. Pollut. 352, 124167. https://doi.org/10.1016/j.envpol.2024.124167.

Wang, Y., Yang, Y., Shi, J., An, W., Lyu, T., Zhang, P., 2024. Processes and mechanisms in remediation of aqueous chromium contamination by sulfidated nano-scale zerovalent iron (S-nZVI): experimental and computational investigations. J. Hazard Mater. 469, 134031. https://doi.org/10.1016/j.jhazmat.2024.134031.

Wei, H., He, Y., Jiang, J., Song, X., Lou, W., Zhang, Z., Zhang, K., 2024. Enhanced transport of K-nZVI by bentonite suspensions in porous media. J. Cent. South Univ. 31, 1149–1162. https://doi.org/10.1007/s11771-024-5629-0.

Wu, H., Schwartz, D.K., 2020. Nanoparticle tracking to probe transport in porous media. Acc. Chem. Res. 53, 2130–2139. https://doi.org/10.1021/acs.accounts.0c00408.

Wu, Y., Guan, C.-Y., Griswold, N., Hou, L., Fang, X., Hu, A., Hu, Z., Yu, C.-P., 2020. Zero-valent iron-based technologies for removal of heavy metal(loid)s and organic pollutants from the aquatic environment: recent advances and perspectives. J. Clean. Prod. 277, 123478. https://doi.org/10.1016/j.jclepro.2020.123478.

Xie, Y., Zhang, M., Ma, L., Du, T., Zhou, D., Fu, M.-L., Yuan, B., Li, X., Hu, Y., 2024. Overlooked encounter process that affects physical behaviors of stabilized nanoscale zero-valent iron during *in situ* groundwater remediation. J. Hazard Mater. 461, 132547. https://doi.org/10.1016/j.jhazmat.2023.132547.

Xu, J., Li, H., Lowry, G.V., 2021. Sulfidized nanoscale zero-valent iron: tuning the properties of this complex material for efficient groundwater remediation. Acc. Mater. Res. 2, 420–431. https://doi.org/10.1021/accountsmr.1c00037.

Xu, J., Wang, Y., Weng, C., Bai, W., Jiao, Y., Kaegi, R., Lowry, G.V., 2019. Reactivity, selectivity, and long-term performance of sulfidized nanoscale zerovalent iron with different properties. Environ. Sci. Technol. 53, 5936–5945. https://doi.org/10.1021/acs.est.9b00511.

Xu, Y., Zanli, B.L.G.L., Chen, J., 2024. New consideration on the application of nano-zero-valent iron (nZVI) in groundwater remediation: refractions to existing technologies. J Nanopart Res 26, 11. https://doi.org/10.1007/s11051-023-05919-8.

Yao, K.-M., Habibian, M.T., O'Melia, C.R., 1971. Water and waste water filtration. Concepts and applications. Environ. Sci. Technol. 5, 1105–1112. https://doi.org/10.1021/es60058a005.

Yusuf, E.O., Amber, I., Officer, S., Oluyemi, G.F., 2024. Transport of nanoparticles in porous media and associated environmental impact: a review. Journal of Engineering Research. https://doi.org/10.1016/j.jer.2024.01.006.

Zafar, A.M., Javed, M.A., Hassan, A.A., Mohamed, M.M., 2021. Groundwater remediation using zero-valent iron nanoparticles (nZVI). Groundwater for Sustainable Development 15, 100694. https://doi.org/10.1016/j.gsd.2021.100694.

Zhang, T., Lowry, G.V., Capiro, N.L., Chen, J., Chen, W., Chen, Y., Dionysiou, D.D., Elliott, D.W., Ghoshal, S., Hofmann, T., Hsu-Kim, H., Hughes, J., Jiang, C., Jiang, G., Jing, C., Kavanaugh, M., Li, Q., Liu, S., Ma, J., Pan, B., Phenrat, T., Qu, X., Quan, X., Saleh, N., Vikesland, P.J., Wang, Q., Westerhoff, P., Wong, M.S., Xia, T., Xing, B., Yan, B., Zhang, L., Zhou, D., Alvarez, P.J.J., 2019. In situ remediation of subsurface contamination: opportunities and challenges for nanotechnology and advanced materials. Environ. Sci.: Nano 6, 1283–1302. https://doi.org/10.1039/C9EN00143C.

Zhu, F., Li, T., Liu, J., 2024. Transport of nZVI/copper synthesized by green tea extract in Cr(IV)-contaminated soil: modeling study and reduced toxicity. Environ. Sci. Pollut. Res. 31, 20499–20509. https://doi.org/10.1007/s11356-024-32463-2.

Zhu, F., Yang, Y., Ren, W., Iribagiza, R.M., Wang, W., 2023. Coupling electrokinetic remediation with flushing using green tea synthesized nano zero-valent iron/nickel to remediate Cr (VI). Environ. Geochem. Health 45, 9691–9707. https://doi.org/10.1007/s10653-023-01767-6.

Web references

https://areeweb.polito.it/ricerca/groundwater/software/mnms/.